In-plane orientation control of (001) κ-Ga_2O_3 by epitaxial lateral overgrowth through a geometrical natural selection mechanism

Yuichi Oshima,[1*] Katsuaki Kawara,[2] Takayoshi Oshima,[2] Takashi Shinohe[2]

[1]*Optical Single Crystals Group, National Institute for Materials Science, 1-1 Namiki, 305-0044 Tsukuba, Japan*

[2]*FLOSFIA, Inc., 1-29 Goryoohara, Nishikyo-ku, 615-8245 Kyoto, Japan*

E-mail: OSHIMA.Yuichi@nims.go.jp

Abstract

Vapor phase growth of *c*-plane κ-Ga_2O_3 films has been reported on various substrates such as sapphire, GaN and AlN. However, these films are not single crystalline, but rather a mixture of nanometer-sized in-plane 120° rotational domains. We demonstrate a technique that solves the in-plane rotational domain problem. κ-Ga_2O_3 was grown by epitaxial lateral overgrowth. A SiO_x mask with a striped or dotted-striped pattern was aligned on a *c*-plane sapphire substrate with a TiO_x buffer layer so that the stripe was parallel to the [11$\bar{2}$0] direction of the sapphire. κ-Ga_2O_3 was then grown on the substrate by halide vapor phase epitaxy. Electron backscatter diffraction, X-ray diffraction, transmission electron microscopy, and selective area electron diffraction revealed that the three in-plane orientations of the κ-Ga_2O_3 domains converged into one whose [010] direction was perpendicular to the stripe. The convergence occurred through a geometrical natural selection mechanism.

1. Introduction

Ga_2O_3 is an ultra-wide bandgap semiconductor (E_g = 4.5–5.3 eV),[1-6] and is therefore an attractive candidate for future high-performance power device applications. Ga_2O_3 can crystalize in several different structures.[7] Among them, β-Ga_2O_3 (monoclinic, *C*2/*m*) is thermodynamically the most stable, and the other polymorphs are meta-stable under atmospheric pressure.[7] Since it is possible to produce high-quality β-Ga_2O_3 single crystal substrates from melt-grown bulk crystals,[8-12] β-Ga_2O_3-based power devices have been intensively studied using the high-quality homoepitaxial β-Ga_2O_3 layers, and a promising

performance of β-Ga_2O_3-based devices, such as Schottky barrier diodes (SBDs)[13] and metal–oxide–semiconductor field effect transistors (MOSFETs),[14] has been demonstrated.

However, some meta-stable Ga_2O_3 polymorphs have their own unique properties that β-Ga_2O_3 does not possess.[15, 16] Such properties may be advantageous for power device applications, and therefore make the meta-stable Ga_2O_3 polymorphs attractive candidates. κ-Ga_2O_3 (orthorhombic, *Pna*2_1),[17, 18] the target material in the present work, is one of these meta-stable phases. Note that κ-Ga_2O_3 is also referred to as orthorhombic ε-Ga_2O_3 for historical reasons.[18-20] The bandgap energy of κ-Ga_2O_3 is reported to be 4.9 eV,[6] which is as large as that of β-Ga_2O_3.[1, 2] One of the most attractive qualities of κ-Ga_2O_3 is spontaneous polarization,[21-23] owing to the lack of inversion symmetry with respect to the *c*-plane. Therefore, we can expect the formation of a two-dimensional electron gas (2DEG) at a hetero-interface with such as κ-$(Al_xGa_{1-x})_2O_3$, GaN, and the realization of high-performance power devices that use the 2DEG.[24-25] In addition, κ-Ga_2O_3 is the second most stable phase among the Ga_2O_3 polymorphs under atmospheric pressure, and the transition temperature to β-Ga_2O_3 is as high as approximately 700 °C.[6] This transition temperature is much higher than that of corundum-structured α-Ga_2O_3 (~500 °C),[4, 26] which is also a meta-stable phase, and promising α-Ga_2O_3-based SBDs and MOSFETs have been demonstrated.[27, 28] Therefore, κ-Ga_2O_3-based devices should be more stable during the annealing process in device fabrication, and we can also expect device operation with higher reliability at elevated temperatures compared with the case of the α-Ga_2O_3 counterparts.

To realize device application of κ-Ga_2O_3, it is essential to establish an epitaxial growth technique to produce high-quality κ-Ga_2O_3 epilayers. So far, halide vapor phase epitaxy (HVPE), metal organic chemical vapor deposition (MOCVD), and mist-CVD have mainly been investigated as the growth techniques of κ-Ga_2O_3 films.[6, 29, 30] The growth investigation needs to be conducted on foreign substrates because κ-Ga_2O_3 substrates are not available. So far, successful growth of phase-pure *c*-plane κ-Ga_2O_3 has been reported on various substrates such as sapphire, GaN, and AlN.[6, 29, 30]

However, the *c*-plane κ-Ga_2O_3 films are not single crystalline, but a mixture of in-plane 120° rotational nanometer-sized domains.[18-20] The high density of the walls of such domains interferes with carrier transport, and may be current leakage paths. Accordingly, it is essential

to solve the "in-plane rotational domain problem" to produce single crystalline κ-Ga_2O_3 films which are indispensable for the production of high-performance devices.

The present work shows that it is possible to solve the in-plane rotational domain problem by applying the epitaxial lateral overgrowth (ELO) technique[31-33] to κ-Ga_2O_3 using a mask with an appropriate pattern and crystallographic direction.

2. Experimental methods

κ-Ga_2O_3 was grown by HVPE in a lab-made horizontal quartz reactor at 540 °C under atmospheric pressure.[6, 34] O_2 (>99.99995% pure) and GaCl were supplied as the precursors. GaCl was synthesized in situ upstream in the reactor by the chemical reaction of Ga metal (>99.99999% pure) and HCl gas (>99.999% pure) at 570 °C. In addition to the precursors, HCl gas was also supplied to improve the growth efficiency by suppressing the parasitic gas-phase reaction.[35] The partial pressures of the O_2, GaCl, and HCl supply were 1.25, 0.125, and 0.125 kPa, respectively. N_2 gas (dew point < −110 °C) was used as the carrier gas. The growth rate of a flat *c*-plane κ-Ga_2O_3 film was approximately 11 μm/h under these growth conditions. The growth time was 5 min to 2 h.

κ-Ga_2O_3 was grown on a TiO_x (2-nm-thick)/*c*-plane sapphire substrate with a 40-nm-thick SiO_x mask (Fig. 1). Deposition of the TiO_x buffer layer enabled the growth of *c*-plane κ-Ga_2O_3 on *c*-plane sapphire.[33] TiO_x and SiO_x layers were deposited by RF sputtering. The SiO_x mask was formed by conventional photolithography. Several mask patterns were examined, and they are shown in each part in the results and discussion section.

The morphology of the κ-Ga_2O_3 crystals was observed by scanning electron microscopy (SEM). Phase purity and out-of-plane orientation was checked by XRD 2θ-ω scan. In-plane orientation was investigated by electron backscatter diffraction (EBSD) and XRD ϕ-scan of the *122* diffraction of κ-Ga_2O_3 in skew-symmetric geometry. Crystal structure and behavior of crystal defects on the microscopic scale were examined by transmission electron microscopy (TEM) and selective area electron diffraction (SAED).

3. Results and discussion

3.1 Growth with a dotted mask with triangular lattice pattern

First, the results on a triangular-lattice dot pattern mask (Fig. 2(a)) are presented. The mask was aligned so that a side of a triangle was parallel to the [11$\bar{2}$0] direction of the sapphire (hereinafter denoted as [11$\bar{2}$0]$_{sap}$).

Figure 2(b) presents an SEM image of a sample grown for 30 min. A regular array of hexagonal-shaped islands was observed. Each island was surrounded by {130} side facets. This result indicated that the growth rate of {130} plane was the slowest among those of crystal planes in the [001] zone (i.e., (*hk*0) planes) under the growth conditions used in the present work. The diameter of an island was approximately 30 μm, which was much larger than that of the mask window (5 μm). This meant that a large part of the κ-Ga_2O_3 island was in a laterally overgrown area on the mask.

Figure 3 shows the XRD 2θ-ω scan profile of the sample. Only diffraction peaks from the *c*-planes of κ-Ga_2O_3 and sapphire were observed. Note that diffraction peaks of TiO_x and SiO_x were not detected because the TiO_x layer was extremely thin, and SiO_x mask was amorphous. Thus, the growth of phase-pure *c*-axis oriented κ-Ga_2O_3 was confirmed.

Figure 4(a) shows the orientation map of κ-Ga_2O_3 obtained by EBSD analysis. Laterally grown areas of a κ-Ga_2O_3 island were composed of six relatively large domains with in-plane 120° rotational directions while the window area was a mixture of small in-plane rotational domains (inset of Fig. 4 (a)). Figure 4(b) depicts a schematic of a κ-Ga_2O_3 island showing crystallographic orientations of the domains. <010> was parallel to <1$\bar{1}$00>$_{sap}$.

Figure 5(a) shows a cross-sectional TEM image of a κ-Ga_2O_3 island. The sampling position and observation direction are shown in Fig. 5(b). On the window area, a high density of line contrast along the *c*-axis was observed. The line contrast was proposed to arise from the boundaries of the small in-plane rotational domains. An SAED pattern of this area (Fig. 5 (c)) could not be explained by diffraction from one single crystalline κ-Ga_2O_3. In addition, each diffraction spot was accompanied by a lateral streak, which indicated a small lateral size of the domains. These results support the results of the EBSD analysis and TEM contrast, both of which indicate that the window area was a mixture of small domains with different orientations. However, no contrast showing the existence of 120° rotational domains was observed in the laterally grown area. An SAED pattern of this area (Fig. 5 (d)) agreed with that of single crystalline κ-Ga_2O_3 with <100> incidence. These results indicate that each domain in the laterally gown area was single crystalline. However, the in-plane rotational domain problem was unable to be solved with this mask pattern because in-plane rotational domains with three orientations still existed with virtually the same volume fraction in an

island, and the arrangement of the mask window was isotropic.

3.2 Growth with a dotted-striped mask

Second, the results on a dotted-striped pattern mask (Fig. 6) are presented. The mask was aligned so that a stripe (short period direction) was parallel to $[11\bar{2}0]_{sap}$.

Figure 7(a)–(c) presents SEM images of the samples grown for 5 min to 2 h. First, a hexagonal-shaped island of κ-Ga_2O_3 was formed on each window (Fig. 7(a)). Then, these islands grew vertically and laterally to coalesce with each other to form κ-Ga_2O_3 stripes along $[11\bar{2}0]_{sap}$ (Fig. 7(b)). Finally, these stripes coalesced with each other to form a compact film (Fig. 7 (c)).

Figure 8(a) presents the orientation map of the κ-Ga_2O_3 obtained by EBSD analysis. Single crystalline areas along $[11\bar{2}0]_{sap}$ were observed (shown in red). The volume fraction of the red region was approximately two times greater than that of the other domains (shown in blue and green). Figure 8(b) shows the XRD ϕ-scan profile of κ-Ga_2O_3 *122* diffraction. If the sample was single crystalline κ-Ga_2O_3, only four peaks should appear while twelve peaks should appear if the film was composed of κ-Ga_2O_3 domains with three in-plane 120° rotational orientations with the same volume fraction. [19, 20] In reality, four strong peaks and eight weak peaks were observed. Note that the vertical axis is shown with a linear scale. The strong and weak peaks were attributed to the predominant red domains and other domains, respectively.

Figure 9 shows the proposed mechanism of the in-plane orientation convergence and formation of the domain structure shown in Fig. 8(a). The volume fractions of the three in-plane rotational domains were virtually the same until the coalescence of hexagonal-shaped islands along the short period direction (Fig. 9(a)). After the coalescence, the blue and green domains mutually limited their growth along stripe-parallel direction. In addition, the {130} growth fronts of the blue and green domains shrunk because the red/blue and red/green boundaries of adjacent islands were geometrically aligned so as to approach with each other as the growth proceed on a side of a stripe. (Fig. 9(b)). As a result, the blue and green domains disappeared from the growth front after a while (Fig. 9(c)). Then, only the red domains kept growing laterally (Fig. 9(d)), and finally coalesced with each other to form the observed domain structure (Fig. 9(e)). Note that a longer lateral growth length of κ-Ga_2O_3 stripes is required when the window spacing along the short period direction is wider because blue and green domains grow more during the isolated island growth. From this view point, a shorter window spacing is better to obtain the orientation convergence effectively in a shorter

growth time.

3.3 Growth with a striped mask

Finally, results on a striped pattern mask (Fig. 10) are presented.

Figure 11(a) presents an SEM image of a sample grown for 30 min on a striped mask aligned along $[11\bar{2}0]_{sap}$. A regular array of κ-Ga_2O_3 stripes was observed. The side walls of the stripes were not smooth because of the formation of {130} facets.

Figure 11(b) presents the orientation map of κ-Ga_2O_3 obtained by EBSD analysis. The laterally grown areas were single crystalline because the blue and green domains disappeared within a lateral growth length of approximately 0.5 μm (inset of Fig. 11(b)), while a mixed domain structure was observed on the window areas. The mechanism of orientation convergence here should be similar to that presented in Fig. 9 although the convergence was accomplished in a much shorter lateral growth length. A quick convergence is reasonable if we think of the striped mask as a dotted-striped mask with an infinitely short period along $[11\bar{2}0]_{sap}$ based on the consideration described at the end of Section 3.2.

Figure 12(a) presents an SEM image of a sample grown for 30 min on a striped mask aligned along $[1\bar{1}00]_{sap}$. A regular array of κ-Ga_2O_3 stripes with smooth {130} side facets was observed.

Figure 12(b) presents the orientation map of κ-Ga_2O_3 obtained by EBSD analysis. In contrast to the case of a $[11\bar{2}0]_{sap}$-parallel mask, the laterally overgrown regions were not single crystalline owing to the coexistence of blue and green domains. This was because the blue/green domain boundaries were parallel with each other along the stripe-perpendicular direction, and therefore the geometrical natural selection mechanism did not work to terminate blue or green domains while the red domains were terminated quickly by the geometrical natural selection mechanism.

Figure 13(a) and (b) shows the XRD ϕ-scan profiles of κ-Ga_2O_3 *122* diffraction of the $[11\bar{2}0]_{sap}$-parallel sample (shown in Fig. 11) and $[1\bar{1}00]_{sap}$-parallel sample (shown in Fig. 12), respectively. Note that the vertical axis is shown with a log-scale in contrast to that used in Fig. 8 (b). In the case of the $[11\bar{2}0]_{sap}$-parallel sample (Fig. 13 (a)), four strong peaks and eight weak peaks were observed. The intensity of the strong peaks was approximately 1000 times stronger than that of the weak peaks. The strong and weak peaks were attributed to the single crystalline regions and the window regions, respectively. In the case of the $[1\bar{1}00]_{sap}$-parallel sample (Fig. 13 (b)), eight strong peaks and four weak peaks were observed. The strong peaks were attributed to the laterally grown regions composed of blue and green

domains while the weak peaks were attributed to the window regions.

4. Conclusions

The present work demonstrates the in-plane orientation control of *c*-plane κ-Ga_2O_3 by ELO, and a solution for the in-plane rotational domain problem is established. When a striped or dotted-striped mask was aligned along $[11\bar{2}0]_{sap}$, the in-plane orientation of κ-Ga_2O_3 converged to just one of three orientations during the lateral growth perpendicular to the stripe direction. This occurred through the geometrical natural selection mechanism. As a result, a large single crystalline area was successfully produced. The convergence of in-plane orientation occurred within a lateral growth length of approximately 0.5 μm in the case of a striped mask. Note that κ-Ga_2O_3 domains could behave differently under different growth conditions, and therefore appropriate mask geometry could be different. Although mixed-domain areas still remained on the window areas, it should be possible to eliminate such areas by conducting a second ELO process so that the mixed-domain areas are covered under the second mask. If we use a dotted-mask pattern in the second ELO, we should be able to grow single crystalline κ-Ga_2O_3 islands and to investigate their intrinsic growth behavior without being affected by in-plane rotational domains. These results will strongly promote κ-Ga_2O_3 towards device applications.

Acknowledgments

Part of this work was supported by Innovative Science and Technology Initiative for Security (JPJ004596), ATLA, Japan.

References

1) M. Orita, H. Ohta, M. Hirano and H. Hosono, Appl. Phys.Lett. **77**, 4166 (2000).
2) T. Onuma, S. Fujioka, T. Yamaguchi, M. Higashiwaki, K. Sasaki, T. Masui and T. Honda, Appl. Phys. Lett. **103**, 041910 (2013).
3) D. Shinohara and S. Fujita, Jpn. J. Appl. Phys. **47**, 7311 (2008).
4) Y. Oshima, E. G. Villora, and K. Shimamura, Appl. Phys. Express **8**, 055501 (2015).
5) T. Oshima, T. Nakazono, A. Mukai, A. Ohtomo, J. Cryst. Growth, **359**, 63 (2012).
6) Y. Oshima, E. G. Villora, Y. Matsushita, S. Yamamoto, and K. Shimamura, J. Appl. Phys. **118**, 085301 (2015).
7) R. Roy, V. G. Hill, and E. F. Osborn, J. Am. Chem. Soc. **74**, 719 (1952).
8) H. Aida, K. Nishiguchi, H. Takeda, N. Aota, K. Sunakawa, Y. Yaguchi, Jpn. J. Appl. Phys. **47**, 8506 (2008).
9) A. Kuramata, K. Koshi, S. Watanabe, Y. Yamaoka, T. Masui, and S. Yamakoshi, Jpn. J. Appl. Phys. **55**, 1202A2 (2016).
10) E. G. Víllora, K. Shimamura, Y. Yoshikawa, K. Aoki, N. Ichinose, J. Cryst. Growth **270**, 420 (2004).
11) Z. Galazka, K. Irmscher, R. Uecker, R. Bertram, M. Pietsch, A. Kwasniewski, M. Naumann, T. Schulz, R. Schewski, D. Klimm, and M. Bickermann, J. Cryst. Growth **404**, 184 (2014).
12) K. Hoshikawa, E. Ohba, T. Kobayashi, J. Yanagisawa, C. Miyagawa, Y. Nakamura, J. Cryst. Growth **447**, 36 (2016).
13) K. Sasaki, A. Kuramata, T. Masui, E.G. Víllora, K. Shimamura, and S. Yamakoshi, Appl. Phys. Express **5**, 035502 (2012).
14) M. Higashiwaki, K. Sasaki, T. Kamimura, M.H. Wong, D. Krishnamurthy, A. Kuramata, T. Masui, S. Yamakoshi, Appl. Phys. Lett. **103**, 123511 (2013).
15) K. Kaneko, S. Fujita, and T. Hitora, Jpn. J. Appl. Phys. **57**, 02CB18 (2018).
16) M. B. Maccioni and V. Fiorentini, Appl. Phys. Express **9**, 041102 (2016).
17) H. Y. Playford, A. C. Hannon, E. R. Barney, and R. I. Walton, Chem. Eur. J **19**, 2803 (2013).
18) I. Cora, F. Mezzadri, F. Boschi, M. Bosi, M. Čaplovičová, G. Calestani, I. Dódony, B. Pécz, and R. Fornari, Cryst. Eng. Comm, **19**, 1509 (2017).
19) M. Kracht, A. Karg, J. Schörmann, M. Weinhold, D. Zink, F. Michel, M. Rohnke, M. Schowalter, B. Gerken, A. Rosenauer, P. J. Klar, J. Janek, and M. Eickhoff,

Phys. Rev. Applied **8**, 054002 (2017).

20) H. Nishinaka, H. Komai, D. Tahara, Y. Arata, and M. Yoshimoto, Jpn. J. Appl. Phys. **57**, 115601 (2018).
21) M. B. Maccioni and V. Fiorentini, Appl. Phys. Express **9**, 041102 (2016).
22) F. Mezzadri, G. Calestani, F. Boschi, D. Delmonte, M. Bosi, and R. Fornari, Inorg. Chem. **55**, 12079 (2016).
23) J. Kim, D. Tahara, Y. Miura, and B. G. Kim, Appl. Phys. Express **11**, 061101 (2018).
24) S. B. Cho and R. Mishra, Appl. Phys. Lett. **112**, 162101 (2018).
25) P. Ranga, S. B. Cho, R. Mishra and S. Krishnamoorthy, Appl. Phys. Express **13**, 061009 (2020).
26) S. D. Lee, A. Akikawa, and S. Fujita, Phys. Status Solidi C **10**, 1592 (2013).
27) M. Oda, R. Tokuda, H. Kambara, T. Tanikawa, T. Sasaki, and T. Hitora: Appl. Phys. Express **9**, 021101 (2016).
28) FLOSFIA and Kyoto univ: News release, July 13 (2008). http://flosfia.com/20180713/
29) F. Boschi, M. Bosi, T. Berzina, E. Buffagni, C. Ferrari, R. Fornari, J. Cryst. Growth **443**, 25 (2016).
30) H. Nishinaka, D. Tahara, and M. Yoshimoto, Jpn. J. Appl. Phys. **55**, 1202BC (2016).
31) A. Usui, H. Sunakawa, A. Sakai, and A. A. Yamaguchi, Jpn. J. Appl. Phys. **36**, L899 (1997).
32) Y. Oshima, K. Kawara, T. Shinohe, T. Hitora, M. Kasu, and S. Fujita, APL Mater. **7**, 022503 (2019).
33) Y. Oshima, K. Kawara, T. Oshima, M. Okigawa, and T. Shinohe, Jpn. J. Appl. Phys. **59**, 025512 (2020).
34) Y. Oshima, *Gallium Oxide: Materials Properties, Crystal Growth, and Devices* (Springer Nature, Switzerland AG, 2020) Chapter 11 (ISBN 978-3-030-37152-4).
35) Y. Oshima, K. Kawara, T. Oshima, M. Okigawa, and T. Shinohe, Semicond. Sci. Technol. 35, 055022 (2020).

Figure Captions

Fig. 1. Substrate structure used for ELO of κ-Ga_2O_3.

Fig. 2. (a) Triangular mask pattern used for the ELO of κ-Ga_2O_3. (b) Bird's-eye-view SEM image of κ-Ga_2O_3 islands grown on the mask.

Fig. 3. XRD 2θ-ω scan profile of κ-Ga_2O_3 islands grown on a triangular mask.

Fig. 4. (a) Orientation map of the κ-Ga_2O_3 islands obtained by EBSD analysis. The inset shows a magnified image of a κ-Ga_2O_3 island. (b) Schematic of an average domain structure. Rectangular frames show the unit cell of κ-Ga_2O_3.

Fig. 5. (a) Cross-sectional TEM image of a κ-Ga_2O_3 island. (b) SEM image that shows the sampling position. The green arrow shows the direction from which TEM observation was performed. (c), (d) SAED patterns of the window area and laterally grown area, respectively.

Fig. 6. Dotted-striped mask pattern used for the ELO of κ-Ga_2O_3.

Fig. 7. Bird's-eye-view SEM images of κ-Ga_2O_3 grown on the dotted-striped mask for (a) 5 min, (b) 30 min, and (c) 2 h.

Fig. 8. (a) Orientation map of the sample (c) in Fig. 7 obtained by EBSD analysis. Yellow hexagons schematically show the positions of κ-Ga_2O_3 islands upon first coalescence. Orientation of the unit cell in each domain is also shown. (b) XRD ϕ-scan profile of κ-Ga_2O_3 *122* diffraction. Colored dots show to which domain the diffraction belongs.

Fig. 9. Mechanism of in-plane orientation convergence on a dotted-striped mask.

Fig. 10. Striped mask pattern used for the ELO of κ-Ga_2O_3.

Fig. 11. (a) Bird's-eye-view SEM image and (b) orientation map of κ-Ga_2O_3 grown on the striped mask aligned along $[11\bar{2}0]_{sap}$ obtained by EBSD analysis. The inset shows a magnified image of a κ-Ga_2O_3 stripe.

Fig. 12. (a) Bird's-eye-view SEM image and (b) the EBSD orientation map of κ-Ga_2O_3 grown on the striped mask aligned along $[1\bar{1}00]_{sap}$. The inset shows a magnified image of a κ-Ga_2O_3 stripe.

Fig. 13. XRD ϕ-scan profiles of κ-Ga_2O_3 samples grown on (a) a $[11\bar{2}0]$ oriented striped mask, and (b) a $[1\bar{1}00]$ oriented striped mask. Note that the vertical axis is shown with a log-scale. Colored dots show to which domain the diffraction belongs.

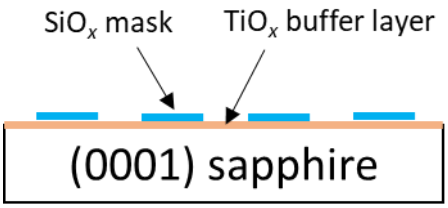

Fig. 1

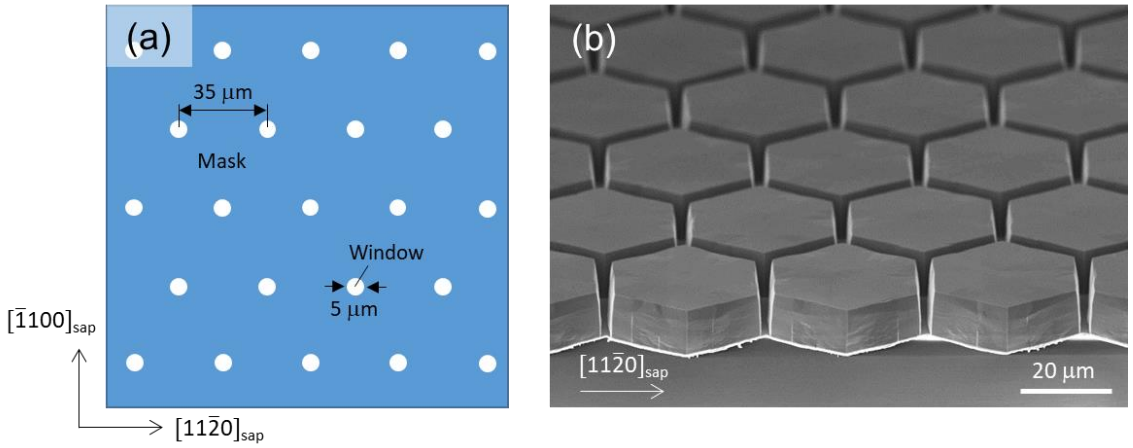

Fig. 2

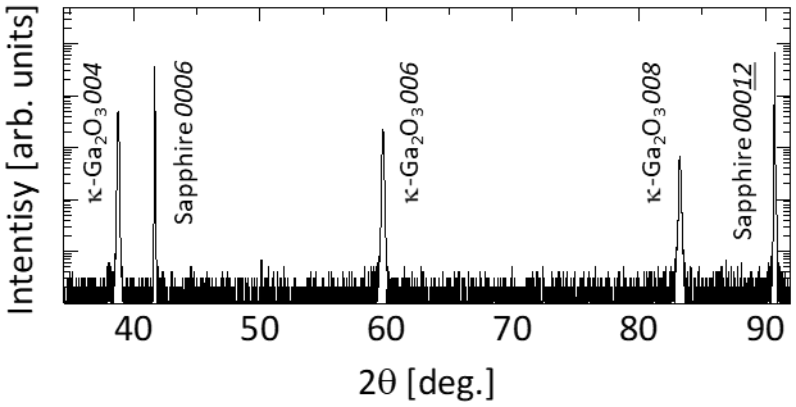

Fig. 3

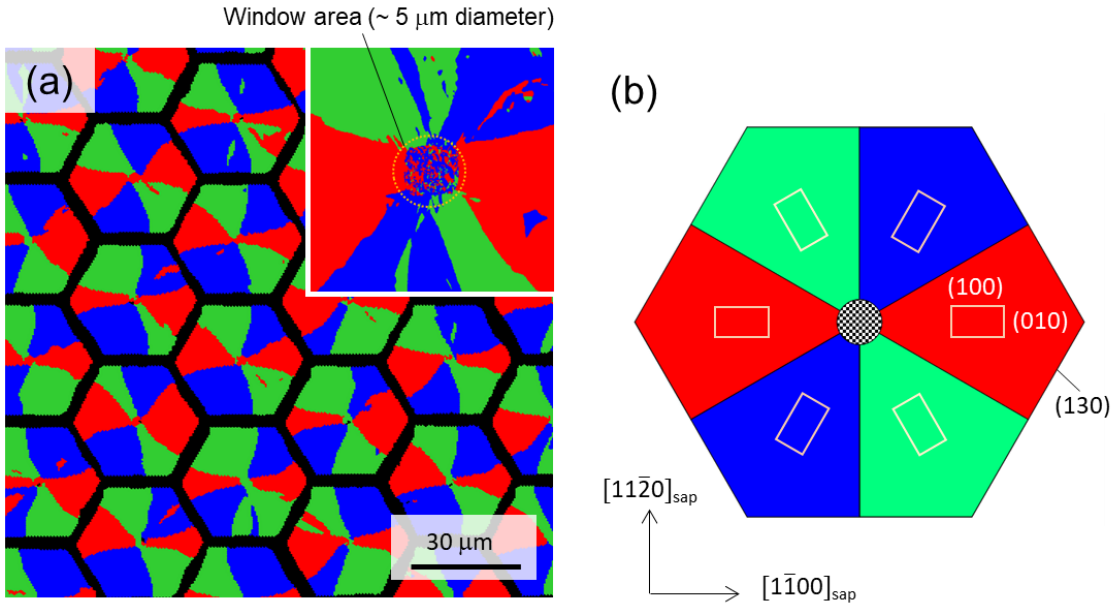
Window area (~ 5 μm diameter)
(a)
30 μm
(b)
(100)
(010)
(130)
[11$\bar{2}$0]$_{sap}$
[1$\bar{1}$00]$_{sap}$

Fig. 4

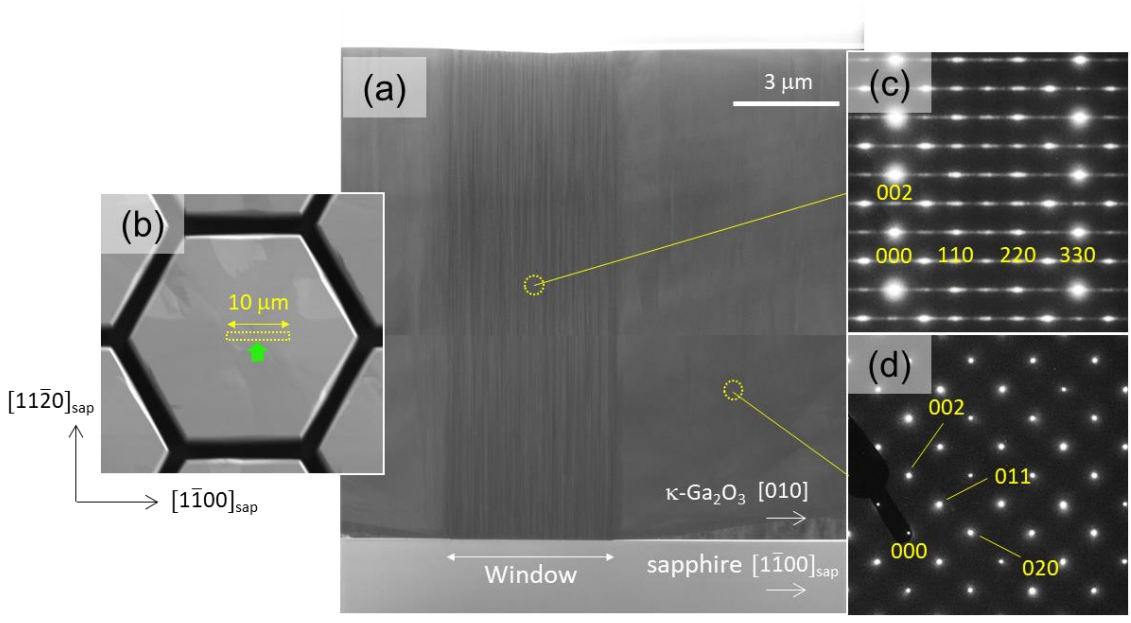
(a)
3 μm
(b)
10 μm
[11$\bar{2}$0]$_{sap}$
[1$\bar{1}$00]$_{sap}$
κ-Ga$_2$O$_3$ [010]
Window
sapphire [1$\bar{1}$00]$_{sap}$
(c)
002
000 110 220 330
(d)
002
011
000
020

Fig. 5

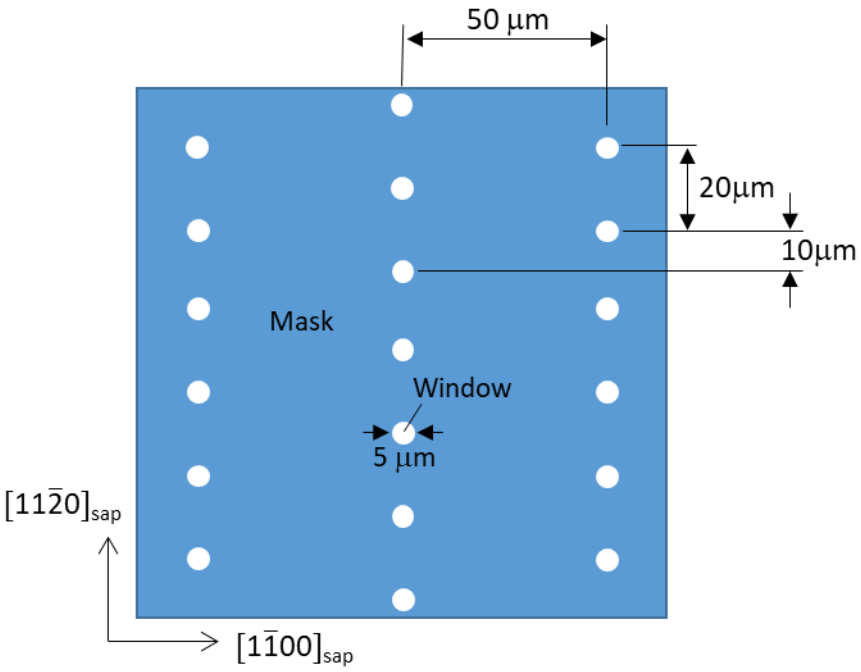
50 µm
20µm
10µm
Mask
Window
5 µm
[11$\bar{2}$0]sap
[1$\bar{1}$00]sap

Fig. 6

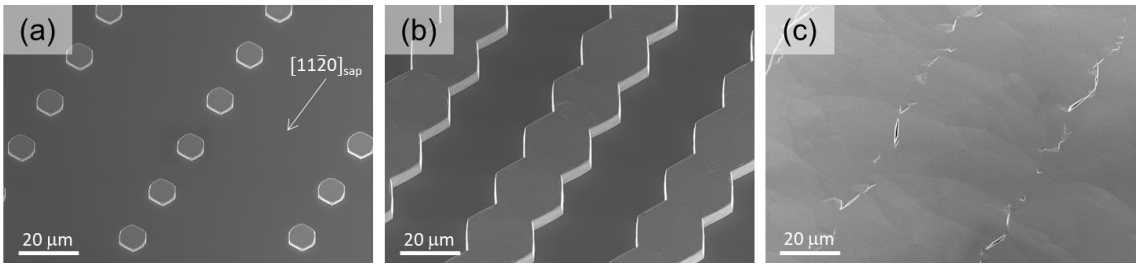
(a)
[11$\bar{2}$0]sap
20 µm
(b)
20 µm
(c)
20 µm

Fig. 7

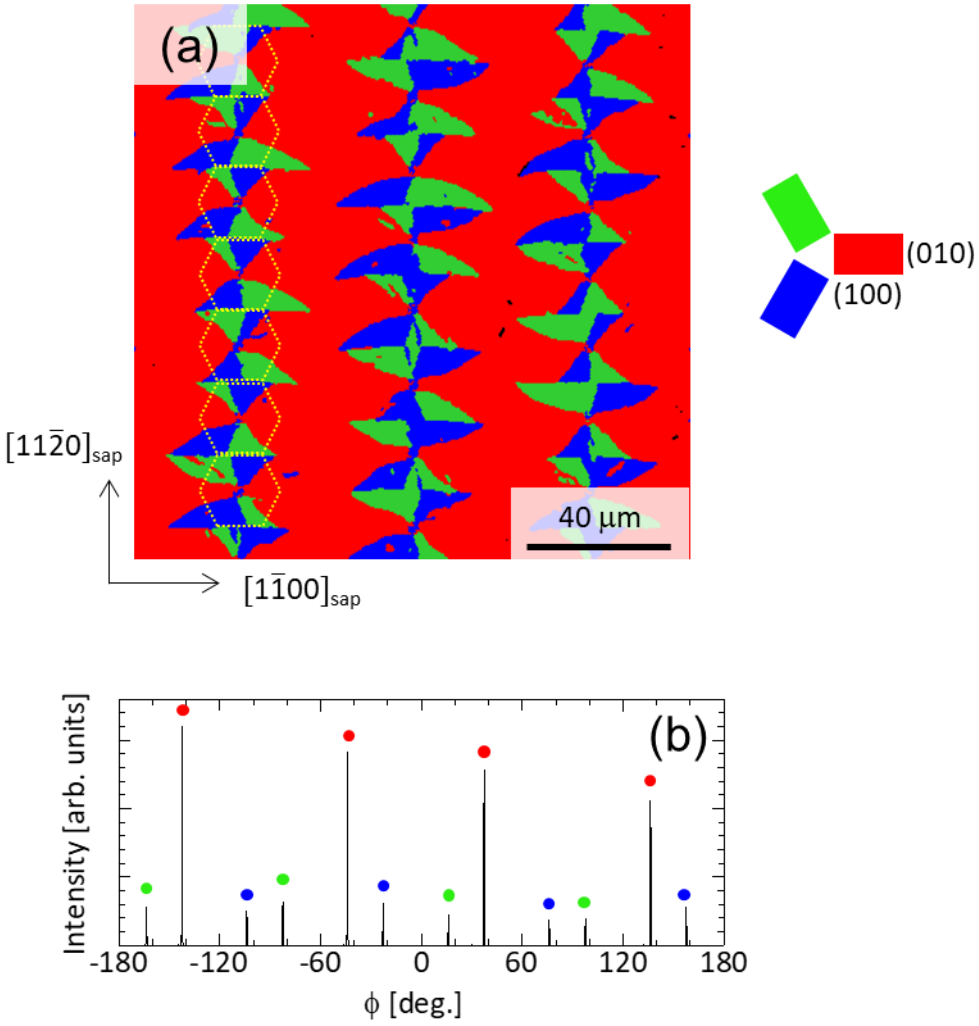
(a)
40 μm
(010)
(100)
[11$\bar{2}$0]sap
[1$\bar{1}$00]sap
(b)
Intensity [arb. units]
-180
-120
-60
0
60
120
180
ϕ [deg.]

Fig. 8

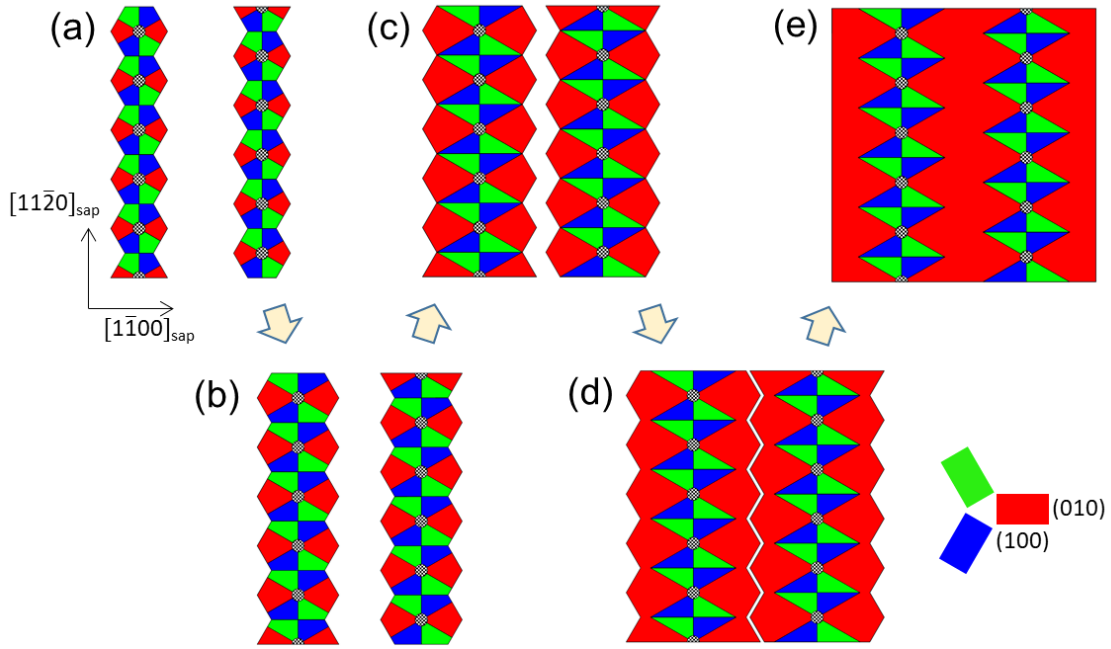

Fig. 9

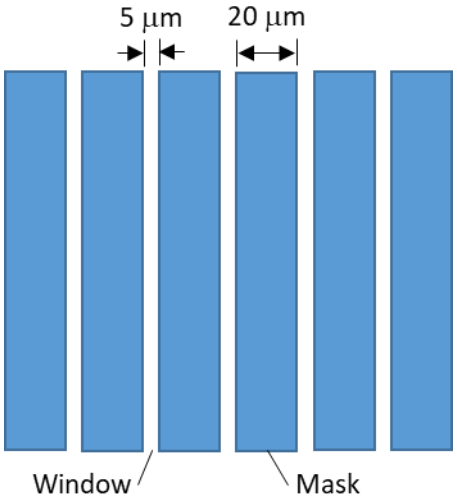

Fig. 10

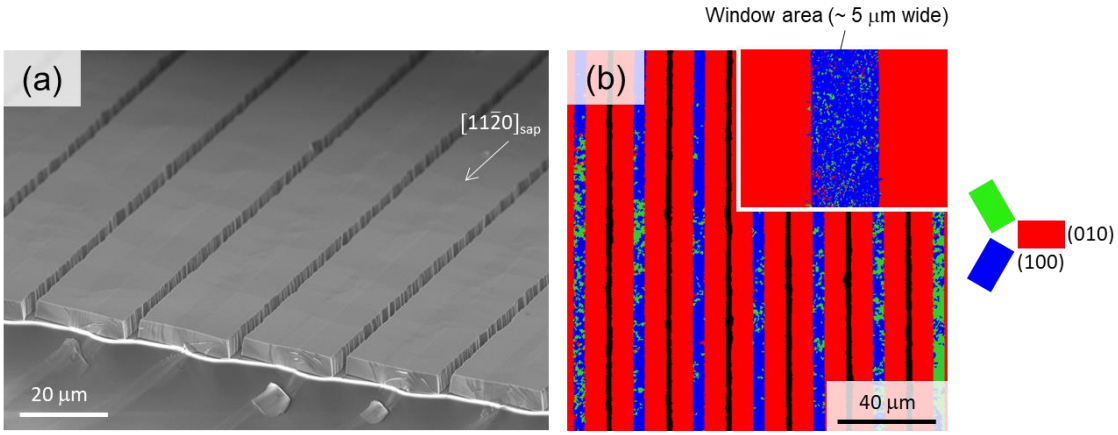
(a)
$[11\bar{2}0]_{sap}$
20 μm
(b)
Window area (~ 5 μm wide)
40 μm
(010)
(100)

Fig. 11

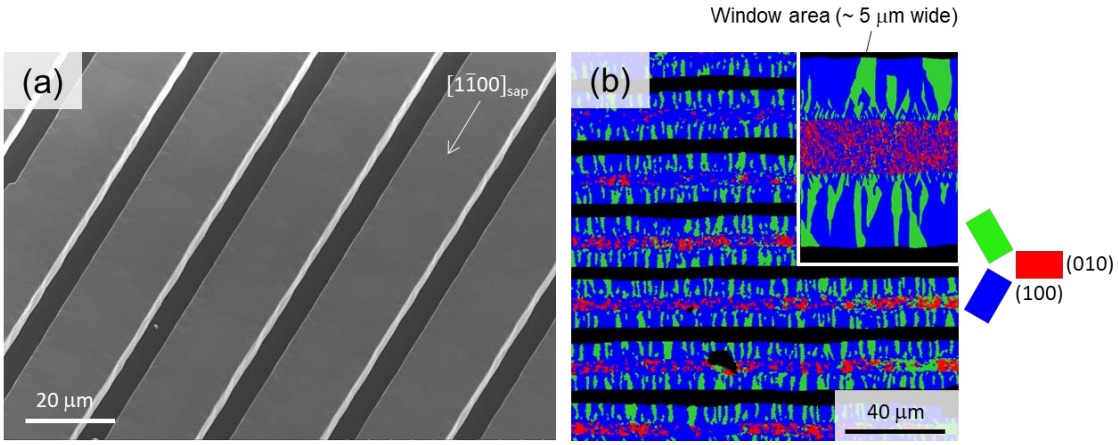
(a)
$[1\bar{1}00]_{sap}$
20 μm
(b)
Window area (~ 5 μm wide)
40 μm
(010)
(100)

Fig. 12

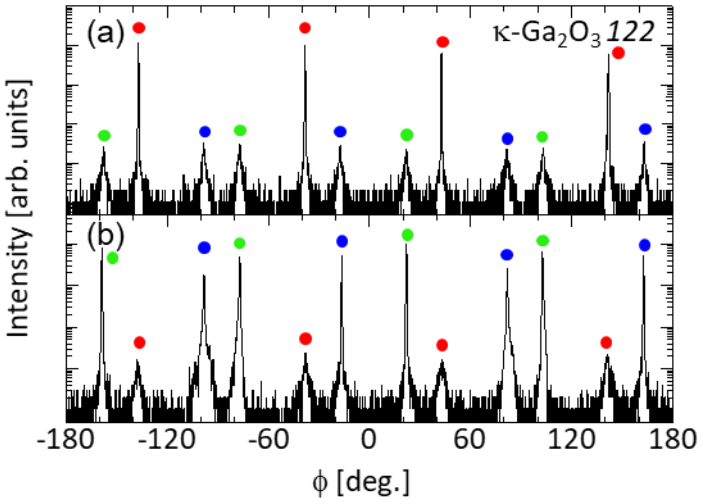

Fig. 13